Int. J. Electrochem. Sci., 8 **(2013)** 369 - 389

International Journal of
ELECTROCHEMICAL
SCIENCE
www.electrochemsci.org

Electrochemical Functionalization of a 316L Stainless Steel Surface with a 11-mercaptoundecanoic Acid Monolayer: Stability Studies

Hesam Dadafarin, Evgeny Konkov and Sasha Omanovic[*]

Department of Chemical Engineering, McGill University, 3610 University Street, Montreal, Quebec, H3A 0C5, Canada
[*]E-mail: sasha.omanovic@mcgill.ca

Received: 5 October 2012 / *Accepted:* 28 November 2012 / *Published:* 1 January 2013

A self-assembled monolayer (SAM) of 11-mercaptoundecanoic acid (MUA) was formed on a 316L stainless steel (SS) surface, using a cyclic potentiodynamic electrochemical technique (cyclic voltammetry). The presence of the formed monolayer was confirmed by polarized modulation infrared reflection adsorption spectroscopy (PM-IRRAS), contact angle (CA), ellipsometry, and X-ray photoelectron spectroscopy (XPS). The stability of the monolayer was investigated by PM-IRRAS, CA and electrochemical impedance spectroscopy (EIS). XPS showed that the MUA is attached to the 316L SS surface mostly through the sulfur atom, but some MUA molecules are also attached to the surface through both the thiol and carboxylate groups. PM-IRRAS demonstrated that the formed SAM is semi-ordered. The SAM was stable in a corrosive environment (phosphate buffer saline, PBS) for seven days, and also withstood the exposure to elevated temperatures and fluid shear stress. EIS results revealed that the SAM also inhibited general corrosion of 316L SS over a period of seven days of constant immersion in PBS, with an average inhibition efficiency of 94%.

Keywords: Self-assembled monolayer; Stainless Steel; Mercaptoundecanoic acid; Electrochemical surface functionalization; Monolayer stability, Corrosion inhibition

1. INTRODUCTION

316L stainless steel (SS) is one of the most widely used materials of construction. Its application spans from the use as a construction material for the equipment employed in the (petro)chemical industry [1], the food and pharmaceutical industries [1, 2], to its use in medicine [3-5]. The advantages of SS over other metals and alloys are its relatively satisfactory corrosion resistance, high mechanical stability, and relatively low cost. However, in some specific biotechnological and

biomedical applications, there are also certain disadvantages associated with the use of SS. Those are mainly related to the physicochemical properties of its surface that provoke negative microorganisms/surface, protein/surface and cell/surface interactions. This may lead to the surface 'fouling' and bacteria adhesion. In the case of the use of SS as a biomedical implant (*e.g.* a coronary stent), this could lead to platelet adhesion and subsequent blood clotting, release of toxic chromium and nickel ions (due to the corrosion of the surface), and even corrosion-induced breakdown (failure) of the SS implant [5-9]. In order to minimize these drawbacks and render the SS surface more corrosion resistant, less susceptible to fouling and/or more biocompatible (depending on its application), modification of the SS surface (*i.e.* its functionalization) has commonly been employed [10-12].

Ultra-thin organic films, such as self-assembled monolayers (SAMs) and Langmuir-Blodgett (LB) films, have been used to modify SS surfaces [13-19]. SAMs are mostly preferred over LB films owing to their ease of fabrication, controlled thickness, and the flexibility to provide tunable functional groups (*e.g.* CH_3, NH_2, COOH) [20].

Alkanethiol SAMs have most commonly been used on model metal surfaces, especially gold [21-28], silver [29], and platinum [30], since the sulfur head group has proven to bind strongly to these surfaces. However, only a few studies on forming alkyl-based SAMs on SS have been published, which is due to the difficulty of forming SAMs on SS. This is because of the high heterogeneity of the SS surface and the presence of an oxide surface film, both of which hamper the formation of stable SAMs on the SS surface. Nevertheless, several methods for the formation of SAMs on SS have been suggested, such as a simple immersion method [14, 31], electrochemical activation [17-19], plasma treatment [15], and thermal pretreatment [16].

The stability of SAMs on surfaces is of great importance for practical applications of SAM-functionalized materials. Although there are numerous studies on the stability of SAMs on gold [24, 32-37], only a few studies have been conducted on the stability of SAMs on SS. Shustak et al. formed decanoic, myristic and palmitic acid SAMs on 316L SS, and reported no significant change in the infrared spectra of the SAMs after seven days, and the authors concluded that the formed SAMs were stable in air [18]. Ruan et al. formed alkyltiol and alkylamine SAMs on 316L SS, and they used X-ray photoelectron spectroscopy (XPS) to verify the oxidative state of the thiol-surface bond. The authors reported that the bond was not oxidized after 4 and 24 hours at ambient conditions (no stability measurements in an electrolyte were reported) [17]. However, contact angle values of the OH-terminated SAM-modified surface varied significantly during the first 10 hours of study. Similar variation in contact angle values of 11-mercapto-1-undecanol SAM on SS was observed by Mahapatro et al. and the authors concluded that the SAM was not stable under ambient conditions (no stability measurements were done in a solution) [15]. In another study by Mahapatro et al., the stability of alkanethiol SAMs on 316L SS in air and in phosphate buffer saline (PBS) was investigated by XPS [15]. The authors reported total desorption of a CH_3-terminated SAM after 14 days under both ambient conditions and in PBS. A similar trend was reported for a COOH-terminated SAM, however, the COOH-terminated SAM desorbed more quickly and by day 14 no metal thiolate peak was observed in XPS spectra. Raman and Gawalt used a solution deposition method to form several alkanoic acid SAMs on a 316L SS surface and measured the chemical stability of the monolayers by rinsing and

sonication in tetrahydrofuran (THF), water and ethanol [38]. The authors reported that the monolayers were stable. In order to verify the mechanical stability of the SAMs, the authors performed a linear adhesion test with Scotch tape 237, and they reported an adhesion strength value of 37 oz in^{-1} [16, 38]. Kaufmann et al. successfully bound methyl and carboxylic acid-terminated phosphonic acids to 316L SS and they used XPS and contact angle (CA) measurements to verify the stability of the SAMs in tris-buffered saline (TBS) at pH = 7.4 on mechanically polished and electropolished samples [14]. The authors concluded that the COOH-terminated SAM was more stable on the surface than the CH_3-terminated SAM [14].

We have recently developed a simple, low-cost, environmentally-friendly, and rapid method to electrochemically form alkanethiol SAMs on 316L SS [39]. In this study, we report on the stability of a COOH-terminated alkanethiol SAM on SS, and on the resulting corrosion stability of the underlying SS surface.

2. MATERIALS AND METHODS

2.1. Sample preparation

316L stainless steel (SS) rod, purchased from McMaster-Carr 9298K131, was cut into round samples (12.7 mm in diameter and 2 mm in thickness). Samples were machine-polished before each SAM binding procedure, with 600, 800 and 1200 grit silicon carbide abrasive paper (Anamet). Each sample was then sonicated successively in deionized water and denatured ethanol for 10 minutes. This step was done to ensure that polishing debris and grease were removed from the surface.

2.2. Mercaptoundecanoic acid monolayer formation

A freshly prepared COOH-terminated SAM-precursor solution, 1mM 11-mercaptoundecanoic acid (MUA) (Aldrich 450561 > 95% purity) in ethanolic 0.1 M $NaClO_4$, was used for the SAM formation. MUA SAMs on SS were formed by utilizing an electrochemical binding method recently developed in our laboratory [39, 40]. The SAM formation process comprised two steps. First, the electrolyte was pre-conditioned by potentiostatic polarization in a standard three-electrode electrochemical cell in which two NiCr electrodes, a working and a counter electrode (8880K32 McMaster-Carr), were immersed in an oxygen-free, MUA-free electrolyte, ethanolic 0.1 M $NaClO_4$ (oxygen was removed by purging the electrolyte with argon). A potentiostat/galvanostat was used to control the electrochemical cell. The potentiostatic polarization of the NiCr working electrodes was performed at -1.0 V vs. saturated calomel electrode (SCE) for 10 minutes (all the potentials in this paper refer to the SCE). Then, the NiCr working electrode was replaced by a SS sample, which served as the working electrode in the second SAM-formation step. Namely, a MUA SAM was electrochemically formed on a freshly-prepared SS sample surface (SS working electrode), by cyclic potentiodynamic polarization of the sample for 22 sweeps (cycles) at a scan rate of 0.05 V s^{-1}, between 0 and -1.8 V, in a 11 mM MUA ethanolic 0.1 M $NaClO_4$ solution. After the SAM formation, each

sample was sonicated for 30 minutes in deionized water and 10 minutes in ethanol to remove physisorbed MUA molecules.

2.3. X-ray photoelectron spectroscopy (XPS)

XPS spectra were collected with an X-ray photoelectron spectrometer equipped with an Al Ka micro-focused monochromator. Energy step size of 0.1 eV was used for high-resolution elemental analysis, and the pass energy for high-resolution scans was 50.0 eV. All binding energies are referenced to the saturated hydrocarbon C 1s peak at 285.0 eV.

2.4. Polarization modulation infrared reflection adsorption spectroscopy (PM- IRRAS)

A Fourier-transform infrared (FTIR) spectrometer equipped with an external polarization modulation module was utilized to record PM-IRRAS spectra. The instrument was equipped with an MCT detector, which was cooled with liquid nitrogen. In order to obtain the highest reflectance amplitude, the polarized IR beam was directed at the samples at an 80° angle to the surface normal. The spectra were averaged over 128 scans at the 3 cm^{-1} resolution.

2.5. Contact angle (CA)

A fully automated goniometer was used to measure static contact angles (CA) and determine the wettability of SS surfaces. After 15 seconds of stabilization of a deionized water droplet on the sample surface, the droplet profiles were captured by the built-in camera and transferred to a computer for further analysis. CA values reported in the paper are the average of a left and right side angle of the droplet. At least three measurements were made on each sample.

2.6. Ellipsometry

Ellipsometry measurements were carried out using an imaging ellipsometer, at a wavelength of λ = 685 nm and angle of incidence of 45°. For ellipsometry measurements, SS samples were polished using 3, 1, 0.5 and 0.25 micron polycrystalline diamond suspension in order to obtain a mirror-like surface finish. Prior to each measurement, optical intensity was optimized by focusing the light beam in X and Y directions. Five areas were measured at different locations on each sample surface, and the average MUA SAM thickness value was calculated. Measurements were performed immediately before (background) and after the MUA binding. The thickness was modeled with a parallel three-layer model using the manufacturer's software. The refractive index and extinction coefficient of the MUA SAM was taken to be n_{MUA} = 1.50 and k_{MUA} = 0, respectively [41, 42].

2.7. Parallel plate flow chamber experiments

A bench-scale apparatus employing a laminar flow chamber (Vacu-Cell VC-LFR-18-H, C&L Instrument, PA, USA) was used to investigate the effect of fluid shear stress on the stability of a covalently bound MUA on a SS surface. The recirculating fluid used in all fluid shear exposure experiments was a phosphate-buffered saline (PBS, 0.16 M NaCl, pH = 7.4) solution. A variable speed peristaltic pump was used to pump the fluid through the flow chamber and produce the required shear stress on the sample surface. A dome pulse dampener was used to eliminate the inherent pulsation in the output flow from the pump. The solution was kept at 37 ºC with a water bath. The PBS solution was continuously pumped through the perfusion chamber at a flow rate of 20.8 ml min^{-1} 72 hours[43, 44]. These experimental conditions were chosen in order to evaluate the SAM stability in an environment closely resembling that of natural blood flow in coronary arteries, since one of the possible uses of SAM modified SS surfaces is for coronary stent applications.

To relatively quantify the amount of MUA remaining on the SS surface after exposure to fluid shear stress for several time intervals, the infrared (IR) integrated intensity of the MUA methylene peaks was determined before and after each experiment. For this reason, a sample surface area of 7 × 7 mm^2 was mapped with a 15X grazing angle infrared (GIR) objective of an FTIR microscope equipped with an MCT detector. Each spectrum was obtained at a 4 cm^{-1} resolution, and averaged over 200 scans. Ten evenly spaced spots (7 × 7 mm^2 area) on the sample surface were marked and scanned with the GIR objective before and after each shear stress experiment. In this manner, spot scanning was done across the entire area exposed to shear stress in order to obtain a representative sample of the initial and final IR absorption spectra. Prior to each scanning, a background scan was collected with a blank, mirror-polished SS sample which was rinsed with deionized water, degreased with ethanol and also cleansed in an ultrasonic bath before the measurement.

2.8. Corrosion stability / electrochemical impedance spectroscopy (EIS)

Evaluation of the corrosion stability of SS samples was performed employing the EIS technique, in a standard three-electrode electrochemical cell connected to a computer-controlled potentiostat/galvanostat/frequency-response-analyzer. A SS sample was connected to a potentiostat as a working electrode, while a graphite rod and SCE were used as a counter and reference electrodes, respectively (PBS, 0.16 M NaCl, pH = 7.4, T = 37 ºC). The impedance response of the SS sample was measured at open circuit potential (OCP), by *ac*-modulating the potential ±10 mV around the applied *dc* potential (OCP) over a frequency range from 100 kHz to 10 mHz.

3. RESULTS AND DISCUSSION

3.1. SAM formation and characterization

The cyclic potentiodynamic method of MUA SAM formation on SS is presented in Figure 1 (main plot). The plot shows a set of cyclic voltammograms (CVs) recorded during the SAM formation.

The potential region positive of ca. -0.8 V represents the electrochemical double-layer region of the SS electrode surface. At the potentials negative of -0.8 V, an increase in cathodic current was recorded as the forward sweep moved to more negative potentials, corresponding to the hydrogen evolution reaction (HER) on the SS electrode surface [45].

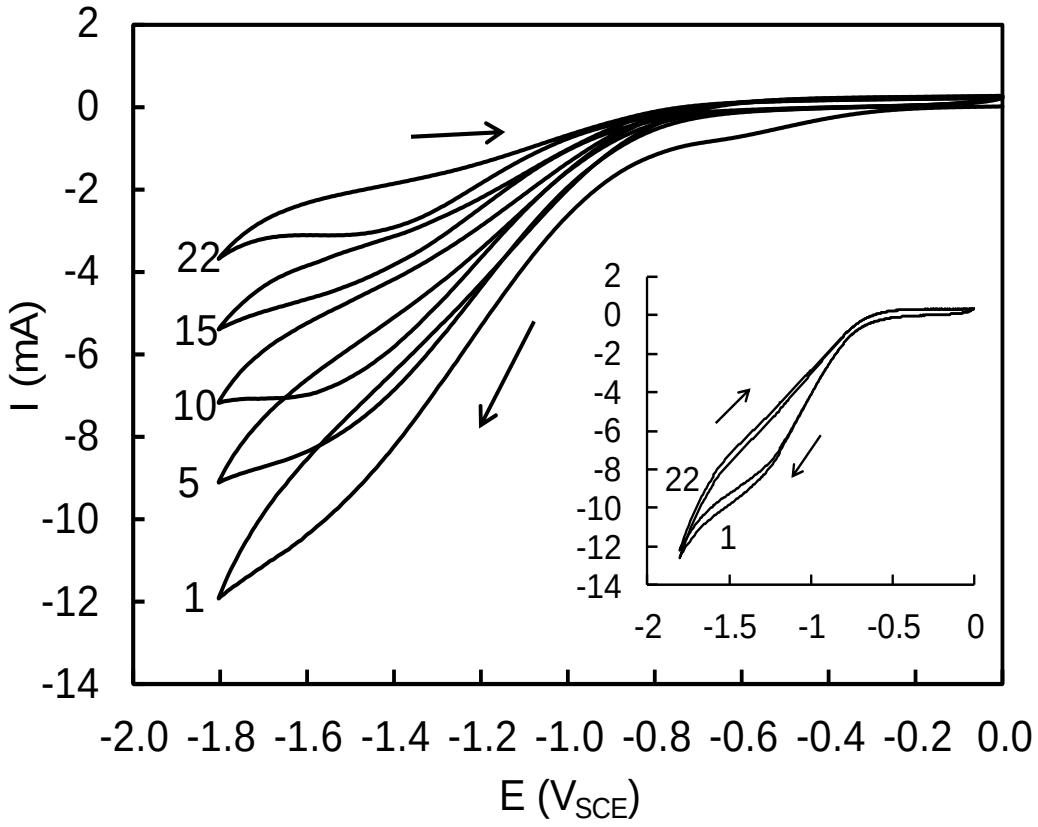

Figure 1. Cyclic potentiodynamic formation (22 sweeps) of a COOH-terminated layer on a 316L-SS surface in ethanolic 0.1 M $NaClO_4$ with 1mM MUA Scan rate was 50 mV s^{-1}. The inset shows the 1st and 22nd sweeps recorded under the same experimental conditions in a MUA-free 0.1M $NaClO_4$ solution (control CVs). The axes titles of the inset plot are the same as those on the main plot.

However, with each subsequent cycle performed, the HER current decreased, indicating the gradual increase in the electrode surface blockage by MUA, *i.e.* the formation of a MUA SAM on the surface. This was also confirmed by a control experiment in which a fresh SS surface was potentiodynamically polarized under the same conditions as in Figure 1 (main plot), but with the exception that the electrolyte did not contain MUA. Consequently, no decrease in the HER current was observed with cyclization (inset to Figure 1), clearly demonstrating that the MUA SAM was formed on the SS surface when the surface was polarized in the MUA-containing electrolyte (main plot, Figure 1).

PM-IRRAS spectra were further recorded in order to confirm the presence of the MUA SAM on the SS surface and valuate its surface structure. Figure 2 shows the infrared spectrum recorded in a wavenumber region corresponding to the stretching vibrations of the $–CH_2$ groups of the MUA alkane

chain. The peaks at 2924 cm^{-1} and 2850 cm^{-1} correspond to the asymmetric ($\nu_{asymm\ CH2}$) and symmetric ($\nu_{sym\ CH2}$) stretching bands of the MUA SAM methylene groups. A highly ordered, densely packed "crystalline" alkanethiol monolayer can be characterized by methylene stretching absorbance wavenumbers of $\nu_{asymm\ CH2} \leq 2918\ cm^{-1}$ and $\nu_{sym\ CH2} \leq 2850\ cm^{-1}$ [46, 47].

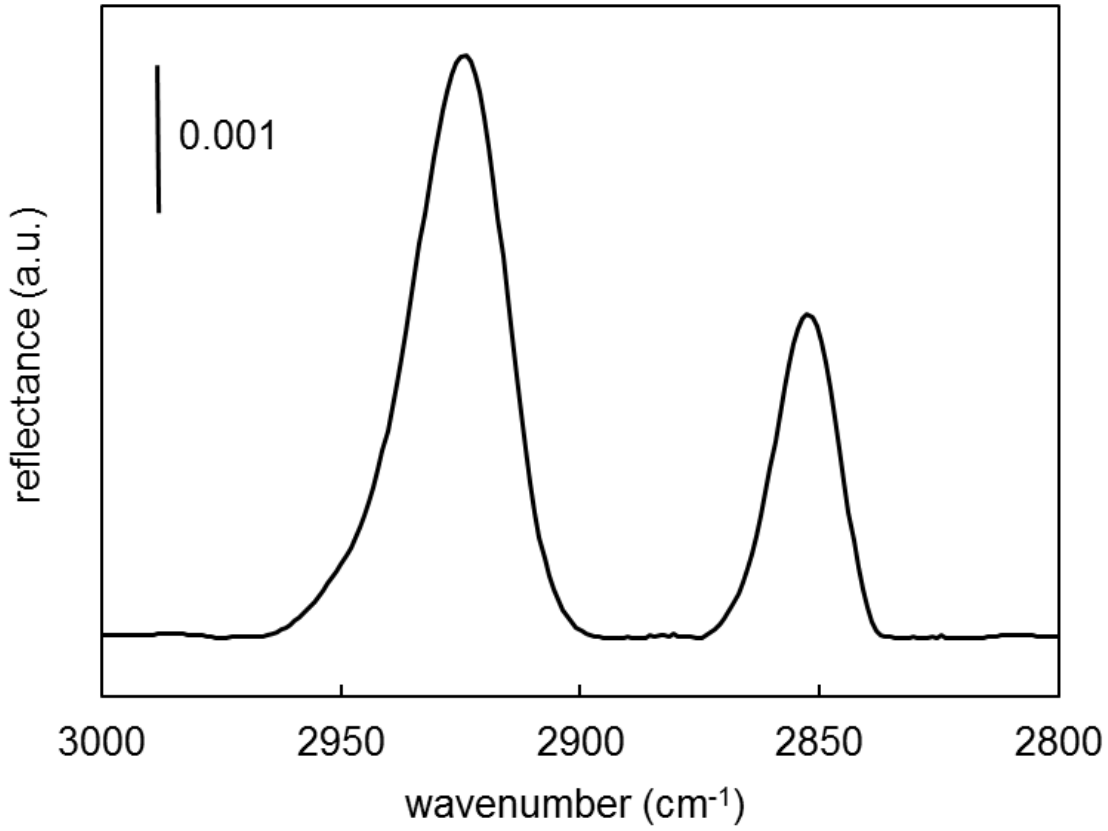

Figure 2. A PM-IRRAS spectrum of methylene asymmetric (2924 cm^{-1}) and symmetric (2850 cm^{-1}) stretches of a MUA SAM formed on a 316L SS surface.

However, such low wavenumbers are typical for well-packed monolayers assembled on very smooth and homogeneous model surfaces, such as monocrystalline gold, while in our case the used SS surface was highly heterogeneous (due to the surface roughness, presence of Mo inclusions, surface oxide film presence), which may have partially caused a slight shift in the methylene band to higher wavenumber (Figure 2) [15]. Another origin of the slightly disordered structure of the formed MUA SAM in Figure 2 could be the surface-binding of some MUA molecules through both the thiol and the carboxylate group (bridging), exposing the hydrophobic ($–CH_2$) chain to the solution [16, 38, 48, 49]. Furthermore, since a COOH-terminated SAM possesses a bulkier terminal group, compared to a CH_3-terminated SAM, there is a higher steric hindrance at the surface. Thus, COOH-terminated SAMs are less likely to form a perfectly well-packed monolayer [14, 50].

Figure 3 – solid line, shows the IR absorption bands of the MUA SAM in the wavenumber region corresponding to the MUA carboxylate and methylene groups. The composite peaks in the

regions of ca. 1650 – 1500 cm^{-1} and 1480 - 1400 cm^{-1} represent the asymmetric and symmetric vibrations of a deprotonated carboxylate terminal group of the MUA SAM ($\nu_{asymm\ COO^-}$ and $\nu_{sym\ COO^-}$, respectively) [23]. Our other experiments on the subsequent chemical modification of a MUA SAM formed on a 316L SS surface with n-hydroxysuccinimide (NHS) [39, 51] revealed that the initially formed MUA SAM was not chemically active, which was determined to be due to the chemical inertness of the terminal $–COO^-$ group. Since sodium ions were present in the MUA precursor electrolyte during the electrochemical MUA SAM formation, the MUA terminal carboxylate group formed a metal complex with Na^+, rendering the MUA SAM chemically inactive [52]. This was also confirmed by our XPS measurement discussed later.

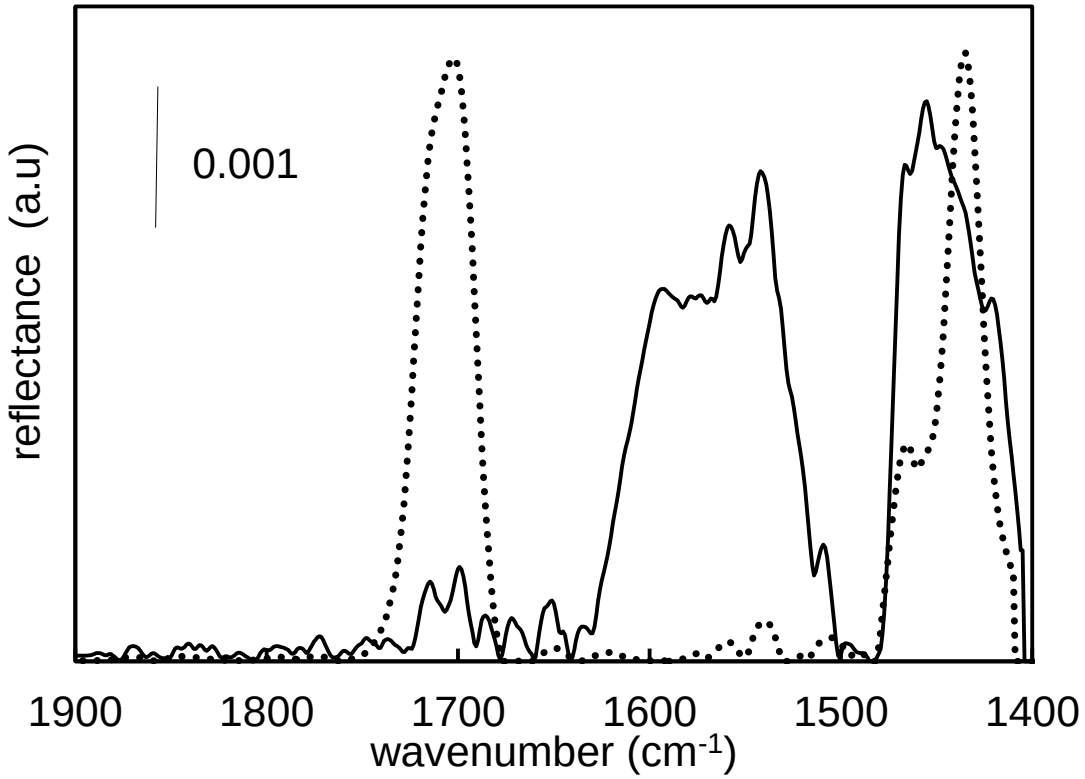

Figure 3. Lower wavenumber region PM-IRRAS spectra of a MUA SAM formed on a 316L SS surface: The solid line represents the response of the MUA SAM immediately after its formation and rinsing, while the dotted line represents the MUA SAM response after the treatment in a phosphoric acid solution.

Thus, to break the complex, and shift the equilibrium to the formation of –COOH, the MUA-modified SS samples were immersed in various aqueous solutions of weak acids (acetic, phosphoric, malonic, citric, boric). Indeed, the composite IR peak initially recorded in the region of ca. 1650 – 1500 cm^{-1} (Figure 3, solid line) disappeared, and a new peak at 1720 cm^{-1} appeared (Figure 3, dotted line). This peak corresponds to the C=O stretching of the free –COOH group, which confirms the breaking of the –COO-Na complex. Also, the symmetric vibration of the $-COO^-$ group initially recorded at 1450 cm^{-1} significantly decreased, and a new vibration at 1430 cm^{-1} appeared. The latter is

assigned to the vibration of the C-O-H bending [53], which further proves the chemical transformation of the –COO-Na complex to a free -COOH. The breaking of the complex was also confirmed by the reaction of the 're-activated' SAM with NHS which proceeded favorably, as evidenced by the appearance of NHS characteristic IR vibrations (not shown here). Among the used weak acids, phosphoric acid (pH = 1.5) was found to destroy the carboxylate-metal complex most efficiently, and was thus used in our further experiments. Also, it is important to mention that the sonication of freshly-prepared MUA-modified SS samples in denatured ethanol, 0.16 M NaCl and 0.1 M NaOH, was unable to remove the carboxylate complexes even after 6 hours of sonication. XPS measurements were done to further prove the presence of MUA on the SS surface through the detection of the MUA sulfur 2p response, Figure 4. As reported in the literature, the spectra of alkanethiols on gold show a 2p response doublet structure centered at 162 and 163.1 eV, which corresponds to the thiol-Au bond. However, after the oxidation of these bonds, other peaks around 165-166 and 167-169 eV appear; they correspond o sulfinates and sulfonates, respectively [27, 54]. The same values are also reported for thiols on iron [55], nickel [56] and silver [57]. Figure 4 (curve *a*) presents the XPS spectrum of the naked SS surface (control), which does not display sulfur peaks. However, when MUA is present on the SS surface, the spectrum displays a doublet peak at 161.8 and 163.5 eV (curve *b*), thus confirming the presence of MUA on the surface and the formation of a sulfur-metal bond. The absence of the 165-166 and 167-169 eV peaks confirms that no oxidized sulfur is present on the surface. Our findings are in agreement with those published in the literature [15, 17].

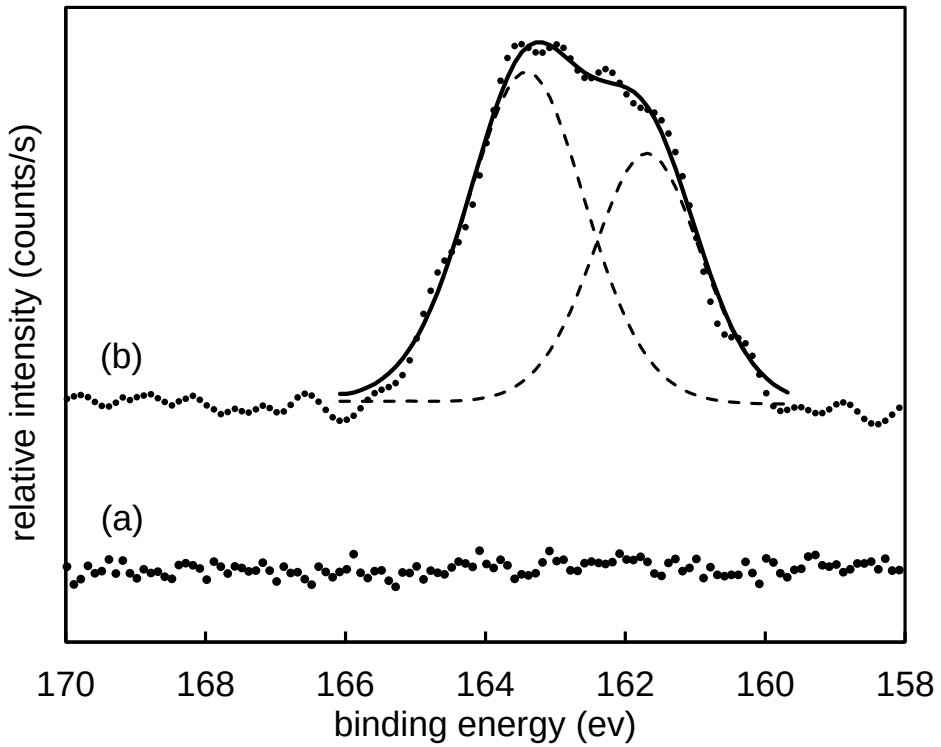

Figure 4. XPS high-resolution sulfur spectra of (*a*) a naked 316L SS surface, and (*b*) a SS surface on which a MUA SAM was electrochemically formed. Dashed lines - the sulfur peak of the MUA-modified sample was deconvoluted into two peaks with maxima at 161.8 and 163.5 eV, and the solid line represents the resulting sum spectrum.

In addition to PM-IRRAS and XPS measurements, contact angle measurements were also done to verify the presence of a MUA SAM on the SS surface and determine the resulting surface wettability. A receding angle of a SAM-modified surface was measured to be 70 ± 1.5° and that of a naked SS surface (control) was 41° ± 2.0°. The relative increase in the contact angle value for the modified surface indicates the presence of a MUA SAM on SS and is in agreement with the findings of Kaufmann *et al*. [14]. Mahapatro et al. [15] reported a CA value of 55.4° ± 21° for a COOH-terminated SAM on 316L SS. On gold substrate, a wide range of CA values have been reported, ranging from 10° to 70° [58, 59]. While most of these studies claimed the formation of a highly-ordered, well packed monolayer, the noticeable variation in CA values may imply that hydrophobic methylene groups of the MUA chain might also be exposed to the electrolyte, which consequently increases the contact angle. As already mentioned before in the text, our opinion is that in the case of a MUA SAM formed electrochemically on SS (Figure 1 to Figure 3), some MUA molecules bind to the SS surface through both the thiol and the carboxylate group, exposing the hydrophobic ($–CH_2$) chain to the solution, which results in a slightly disordered SAM and a higher CA value.

In order to verify the presence of a multilayer on the surface, the thickness of the MUA SAM formed on a SS surface was measured by ellipsometry. Since a SS surface is highly heterogeneous and its chemical, physicochemical, morphological/topographical properties highly depend on the surface treatment, we first needed to determine the optical parameters (refractive index, n_{SS}, and extinction coefficient, k_{SS}) of the SS surface underneath the formed MUA layer. Thus, a freshly prepared SS surface first underwent the same procedure used for forming a MUA SAM, but no MUA precursor was present in the electrolyte. Such a prepared SS surface (control) was assumed to have the same optical properties as the one underneath a MUA SAM, and the resulting parameters were determined to be n_{SS} = 1.899 ± 0.121 and k_{SS} = 3.849 ± 0.168. These values were subsequently used to compute the MUA SAM thickness.

Then, a MUA SAM modified SS surface was mapped with an ellipsometer (area of 350 μm × 350 μm, 0.92 μm per 1 pixel), and the average MUA layer thickness was calculated to be 1.56 ± 0.2 nm. This is very close to the theoretical value of 1.67 nm for an alkanethiol SAM with ten CH_2 groups tilted 30° from the surface normal, which is an angle of a well-ordered SAM [60]. Hence, the ellipsometry measurements confirmed the presence of a MUA *monolayer* on the SS surface in agreement with the PM-IRRAS results (Figure 2). This is important for practical applications of the MUA SAM as a linking layer for covalent immobilization of functional (bio)molecules and / or species (proteins, drugs, nano-particles, etc.) on a SS surface. In the instance of a second MUA monolayer forming on top of the first one, the top (outer) monolayer would easily detach since it would only be physisorbed on top of the first monolayer. On the other hand, the first, immediate surface monolayer is chemically attached to the surface through a metal-sulfur bond (Figure 4) which, as it will be evidenced further in the manuscript, renders the MUA SAM very stable.

3.2. Long-term stability of the MUA SAM on the 316L SS surface

Structural stability of SAMs on surfaces, regardless of their final application, is undoubtedly one of the major requirements. Considering that the substrate surface used in this work is a highly

heterogeneous commercial alloy, 316L SS, and given that the MUA SAM on this surface can be used in various applications (*e.g.* irreversible immobilization of proteins and drugs, improvement of polymer adhesion, regulation of surface wettability, corrosion protection, etc.), it is crucial that the MUA SAM be stable and remain attached to the SS while exposed to various harsh conditions expected in real applications.

In order to assess the stability of the MUA SAM formed on a SS surface (Figure 5 - 7), and also the corrosion stability of the underlying SS surface, the MUA-modified SS samples were kept in a phosphate buffer saline solution (PBS, pH = 7.4, concentration of NaCl = 0.16 M) for a period of seven days, and analyzed daily using different experimental techniques. The PBS solution was renewed every day during the monitoring period.

To relatively quantify the amount of MUA remaining on the SS surface after various immersion periods, the integrated intensity of the symmetric and asymmetric methylene stretches (Figure 2) was determined. As a control, a freshly-prepared SS sample with a MUA SAM was used (day zero), and the integrated intensity of all samples was compared and normalized with respect to that of the control, yielding the values depicted in Figure 5.

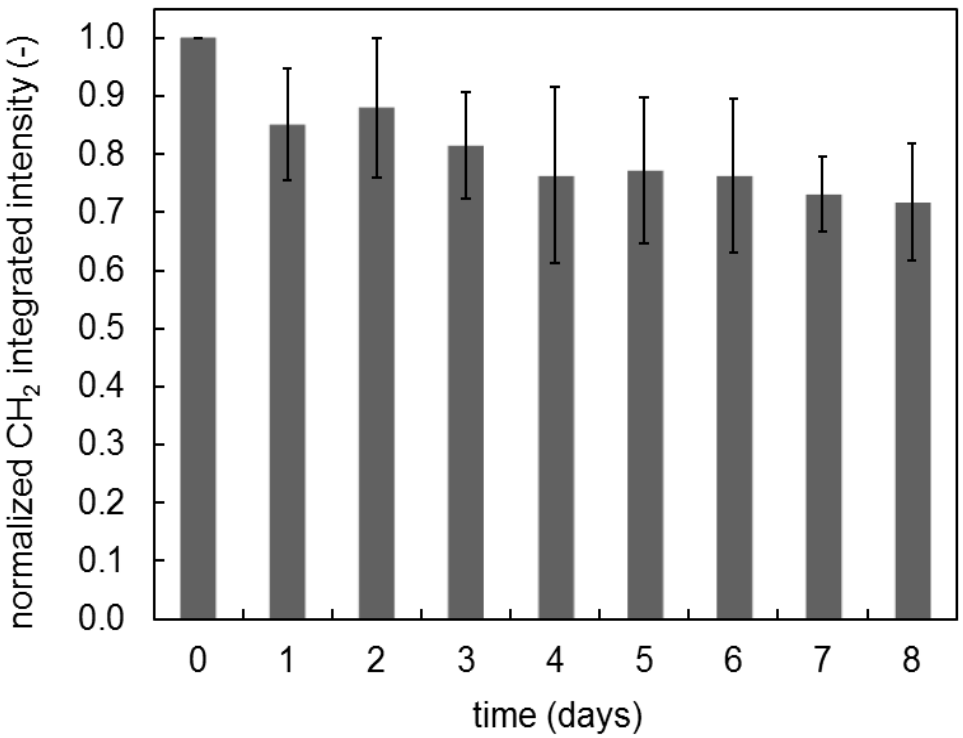

Figure 5. Time dependence of normalized integrated intensity of methylene stretching vibrations in the 2800-3000 cm^{-1} region of a MUA SAM formed on a 316L SS surface, following immersion in PBS (pH = 7.4) during a period of 8 days. The PBS solution was replaced on a daily basis.

The plot demonstrates that the electrochemically formed MUA SAM was quite stable on the SS surface, and after eight days of immersion, ca. 80% of the initial amount was still present on the surface. In order to examine the intensity values for statistical difference between the elapsed days in Figure 5, a set of F-tests was performed to calculate if the variances of the mean readings change with time. Based on the F-

test results, appropriate t-tests were chosen to verify the extent of changes in the mean values of PM-IRRAS integrated intensity on each day. As a result, with a 95% level of confidence, no significant changes have been observed in the PM-IRRAS readings in the last five days of the study ($\alpha = 0.05$, $p > 0.05$). Also, no major structural changes in the SAM were observed during the whole investigated period, since the position of the asymmetric CH_2 stretching peak remained almost constant, 2924±1 cm^{-1}.

Thus, the results in Figure 5 demonstrate that the electrochemical method used to form the MUA SAM on a highly heterogeneous 316L SS surface is quite an efficient method for the preparation of a very stable COOH-terminated alkanethiol SAM. In turn, this SAM could be used as a linker to further functionalize the SS surface (*i.e.* with proteins, drugs, sensing molecules, etc.). Other authors have also investigated short- and long-term stability of SAMs on SS surfaces, and these works were already outlined in the introduction section of the manuscript [14, 15, 17, 18, 38].

The contact angle measurement on a freshly-prepared MUA-modified SS surface, presented earlier in the text, demonstrated that the modified surface is more hydrophobic than the bare SS surface (by ca. 30^o). It would also be interesting to monitor the wettability of both surfaces during a longer period of time, due to its importance in various instances (protein/surface, cell/surface, bacteria/surface interactions, and corrosion protection) [61-63].

In parallel with the PM-IRRAS measurements presented in Figure 5, surface wettability measurements were also done; the obtained data are presented in Figure 6 (separate samples were used in the two sets of experiments). For the MUA-modified SS surface (Figure 6, circles), a ca. 9% drop in the contact angle was recorded after one day of immersion of the samples in the electrolyte, but then the value remained constant during the remaining immersion period ($\alpha = 0.05$, $p > 0.05$). The initial drop indicates that some minor structural changes in the MUA SAM occurred during a short immersion period, rendering the SAM more hydrophilic. This might be due to the re-arrangement and/or orientation of the MUA molecules on the surface to expose the charged and hydrophilic –COOH group more towards the exterior, thus making the entire surface more hydrophilic. The contact angle reading obtained with MUA modified samples in Figure 6 (circles) are in good agreement with those for a COOH-terminated phosphonic acid SAM on electropolished 316L SS, reported by Kaufmann et al. [14]. The authors also concluded that phosphonic acid SAMs were stable on electropolished 316L SS. On the contrary, for mechanically polished surfaces (the same as ours), contact angle readings changed significantly in the first seven days of their study [14]. Moreover, our CA values fall into the range of CA values for a COOH-terminated SAM on 316L SS ($55.4° \pm 21°$) reported by Mahapatro et al. [15], as well.

On the other hand, the contact angle value for the unmodified (naked) SS surface changed significantly during the first day of immersion, from ca. 41^o to ca. 8^o. This sharp decrease indicates that the surface became quite hydrophilic after the first day and remained hydrophilic during the remaining days of constant immersion in PBS. The origin of this behavior is related to the SS surface passivation, *i.e.* to the formation of a thin oxide film on the surface [64]. This film is composed mainly of iron and chromium oxides/hydroxides, which render the surface highly hydrophilic.

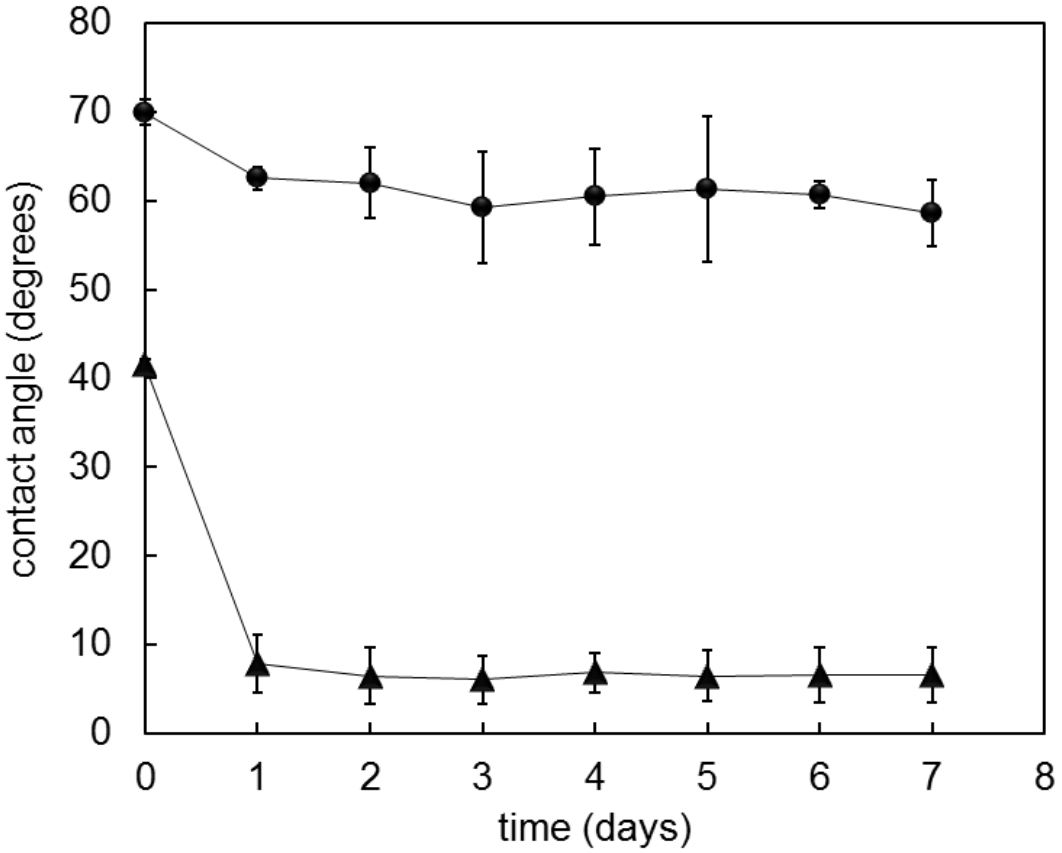

Figure 6. Contact angle values of a (▲) naked 316L SS surface and a (●) 316L SS surface on which a MUA SAM was electrochemically formed. The values at zero day were measured before the samples were immersed in PBS, while the remaining values were measured over a period of 7 days of constant immersion of the samples in PBS.

3.3. Effect of shear stress on the stability of the MUA SAM on the 316L SS surface

A MUA-modified SS substrate was exposed to shear stress to investigate the stability of the formed monolayer under the fluid low conditions. In order to relatively quantify the effect of fluid shear stress on the stability of MUA, ten spots on the MUA-modified 316L SS sample surface were linearly mapped with GIR and the integrated intensity of the methylene vibration was determined before and after the exposure of samples to fluid flow. The normalized integrated intensity value obtained before the fluid flow was 1.00 ±0.15, whereas after 72 hours of flow the value decreased to 0.88 ±0.09. A two-sample *t*-test for equal means was then performed to determine whether the MUA monolayer was affected by the laminar fluid flow. The tests indicated that the MUA monolayer successfully withstood the fluid shear stress, as no significant statistical difference was observed ($\alpha = 0.05$, $p > 0.05$).

3.4. Thermal stability

SAMs formed on SS surfaces should withstand elevated temperatures in certain applications, for example, in cases where the surface functionalization can be used to minimize/control surface

fouling caused by proteins and bacteria (*e.g.* in the dairy/food/pharmaceutical industry). In addition, studying the stability of SAMs at higher temperatures would also provide valuable insight into the stability and strength of the SAM molecule-surface bond, as well as on the intrinsic chemical stability of the SAM.

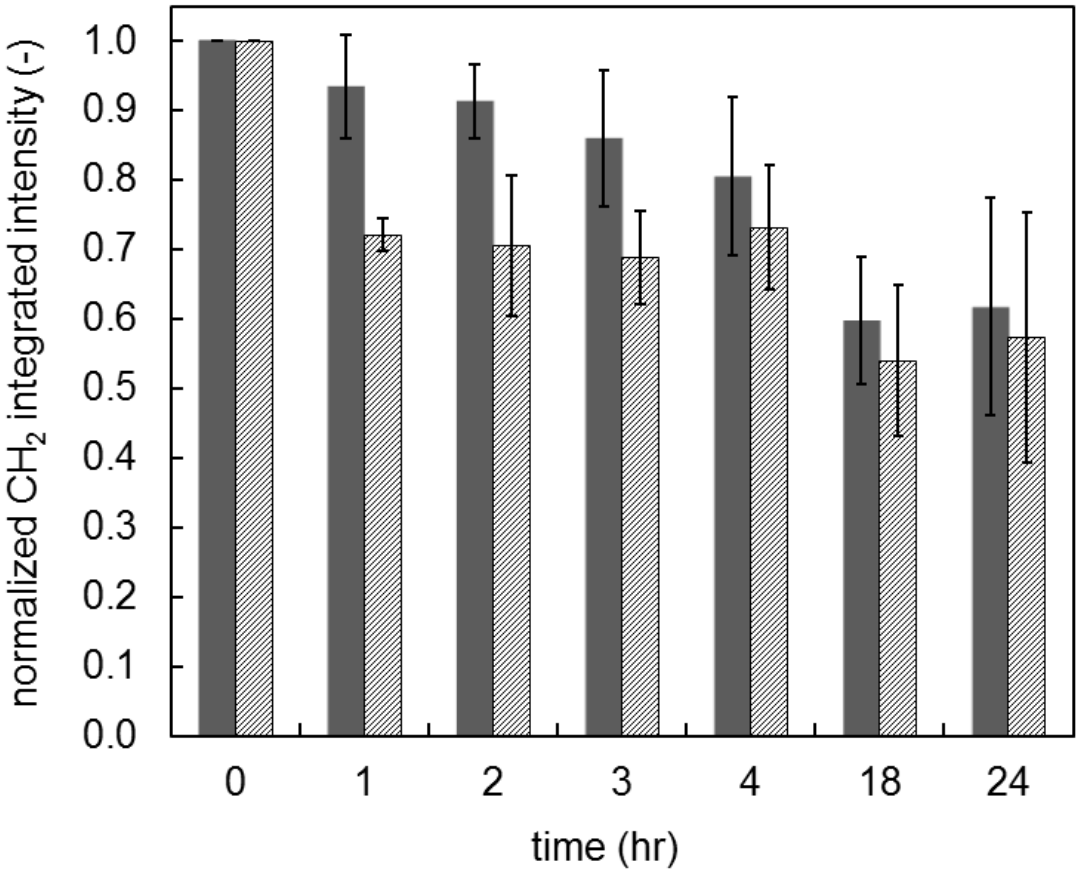

Figure 7. Time dependence of normalized integrated intensity of methylene stretching vibrations in the 2800-3000 cm^{-1} region of a MUA SAM formed on a 316L SS surface, following immersion in PBS (pH = 7.4) during a period of 24 hours at 100 °C (solid bars) and 150 °C (patterned bars).

In order to verify the thermal stability of the MUA SAM formed on the SS surface, SAM-modified samples were kept in an air convection oven at 100°C and 150°C during a period of 24 hours, and the PM-IRRAS spectra were recorded at certain intervals. Figure 7 shows the normalized values of the resulting integrated CH_2 band intensities (Figure 2). The data demonstrate that the amount of MUA present on the surface declines with time. While at 100 ^oC (solid bars) this trend is gradual, at 150 ^oC most of the SAM removal (detachment) occurred during the first hour of surface heat treatment. Nevertheless, after 24 hours of treatment at both temperatures, ca. 60% of the initial amount of MUA SAM still remained on the SS surface, demonstrating a good surface stability of the SAM. Hence, the electrochemical procedure employed to form the SAM is evidently effective and conducive to the formation of strong thiol-surface bonds (Figure 4) which exhibit good stability at the temperatures up

to 150 ^{o}C. This indicates that the MUA-modified SS surfaces could indeed be used in various applications where (shorter-term) high operating temperatures are experienced.

3.5. Effect of the MUA SAM on the SS surface general corrosion properties

316L SS is a standard molybdenum-bearing stainless steel grade which is relatively well resistant to general (uniform) corrosion in the atmosphere and in most corrosive media, due to its high content of chromium and nickel [65]. However, in certain applications where even slight corrosion of 316L SS should be avoided, such as in the case of its use for biomedical implants or in the food, dairy, or pharmaceutical industry, the general corrosion resistance of 316L SS is not satisfactory. Namely, in the more complex corrosive media, *i.e.* in the presence of oxidizing bacteria and/or certain proteins or in the human body, the corrosion resistance of 316L SS decreases significantly, which leads to surface degradation, release of toxic ions (chromium and nickel) into the surrounding environment (e.g. tissue), or complete mechanical fracture of the material [5-9, 66]. Hence, it is important to evaluate the corrosion stability of the MUA-modified SS surfaces, *i.e.* to check whether the surface functionalization results in an increase or a decrease of its corrosion resistance.

In the case of the MUA-modified SS surface, the PM-IRRAS and CA measurements indicated that the MUA SAM is relatively (but not perfectly) structured. Hence, one might hypothesize that the SAM can act as a barrier for the transport of corrosive species (*i.e.* solvated anions) from the bulk electrolyte to the surface, thus basically acting as a corrosion inhibitor. To verify this hypothesis, long-term measurements of the general corrosion stability of the MUA-modified SS surface were done sing electrochemical impedance spectroscopy (EIS) at open-circuit potential (OCP – potential at which the material naturally corrodes). EIS measurements on the unmodified (bare) SS surface were also performed in parallel (control surface). Figure 8a shows the Nyquist spectra of the control (triangles) and MUA-modified (circles) 316L SS surface. The visual inspection of the Nyquist plot indicates that the MUA-modified surface offers a higher corrosion resistance than the control surface, which is evidenced by the larger radius of the partial semi-circle representing the response of the MUA-modified surface (circles) [67-69].

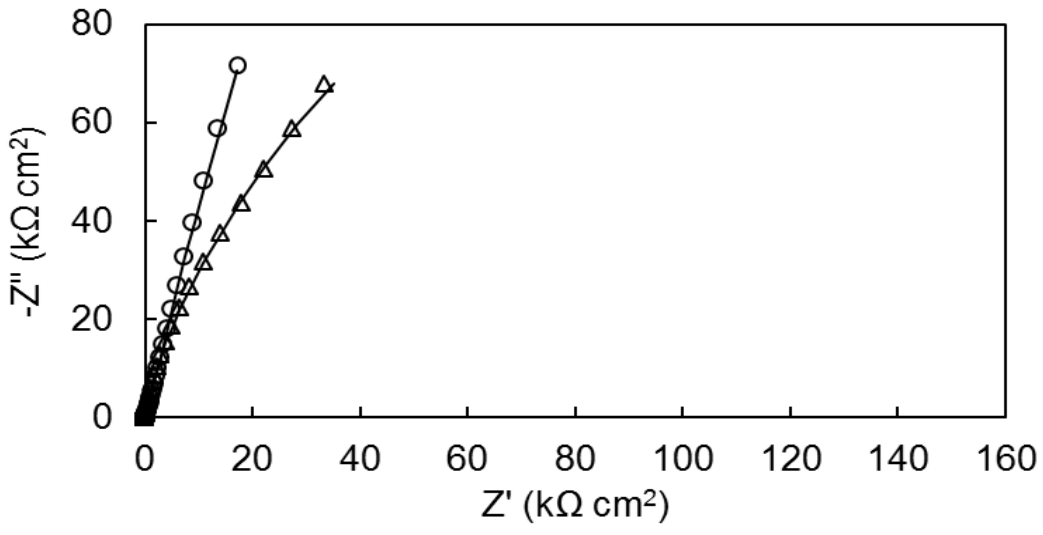

A

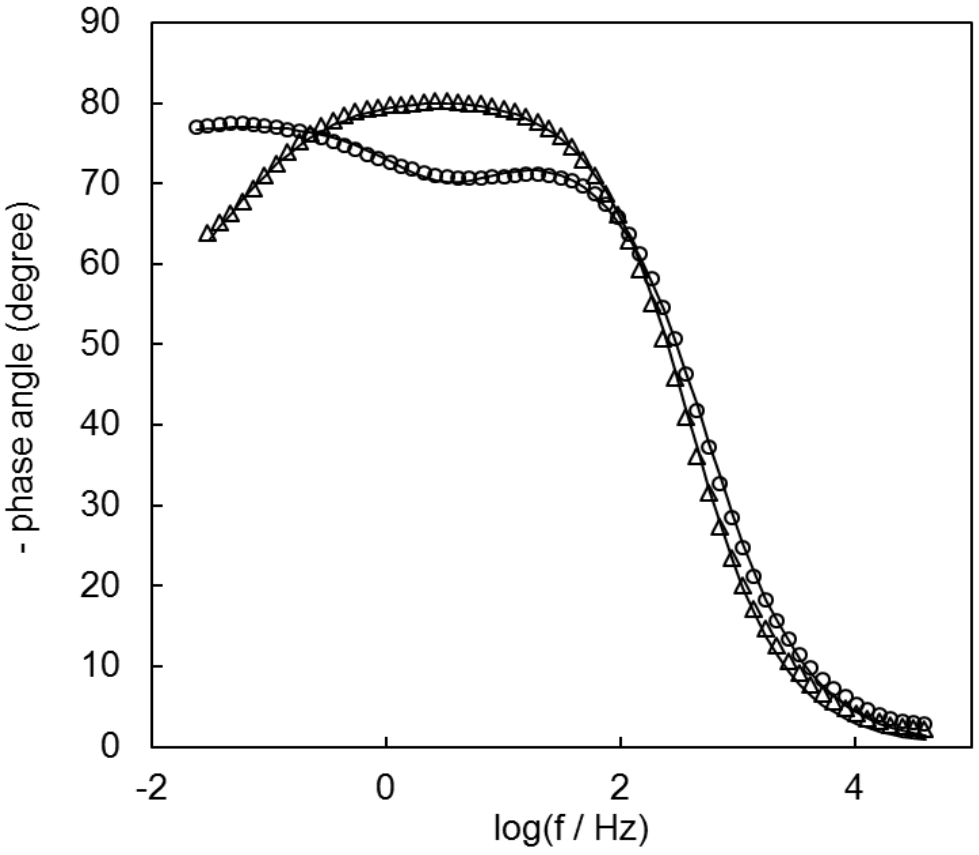

Figure 8. (*a*) Nyquist and (*b*) Bode plot of (Δ) a control (bare) 316L SS surface, and (○) a 316L SS surface modified by a MUA SAM. The data were recorded at OCP after 24 hours of immersion of the samples in PBS, pH = 7.4, at temperature = 37 °C. Symbols signify experimental data and solid lines represent the modeled spectra.

However, to quantify the corresponding corrosion resistance increase, the EIS spectra were modeled by an appropriate equivalent electrical circuit (EEC) model. The same EIS data presented in the form of a Bode plot (Figure 8b) evidence that the spectrum of the control surface (triangles) displays one time constant with a possible contribution of the Warburg (mass-transport) process at low frequencies. On the other hand, the spectrum of the MUA-modified surface (circles) resembles the behavior of a system with two time constants. Hence, the two EIS spectra were correspondingly modeled using the EEC in Figure 9a and b, respectively.

In this figure, R_{el} is the electrolyte resistance measured between the working electrode (samples) and the reference electrode, CPE_1 is a constant-phase element representing the combination of the electrochemical double layer and passive film capacitance, R_1 is the charge transfer resistance, W is Warburg impedance related to diffusion of charged species (in this case through the passive oxide film formed on the naked SS surface), R_2 and CPE_2 are the pseudo-resistance and pseudo-capacitance of the MUA SAM. The sum of R_1 and R_2 represents the total resistance related to the kinetics of corrosion reactions occurring on the SS surface, *i.e.* the total corrosion resistance.

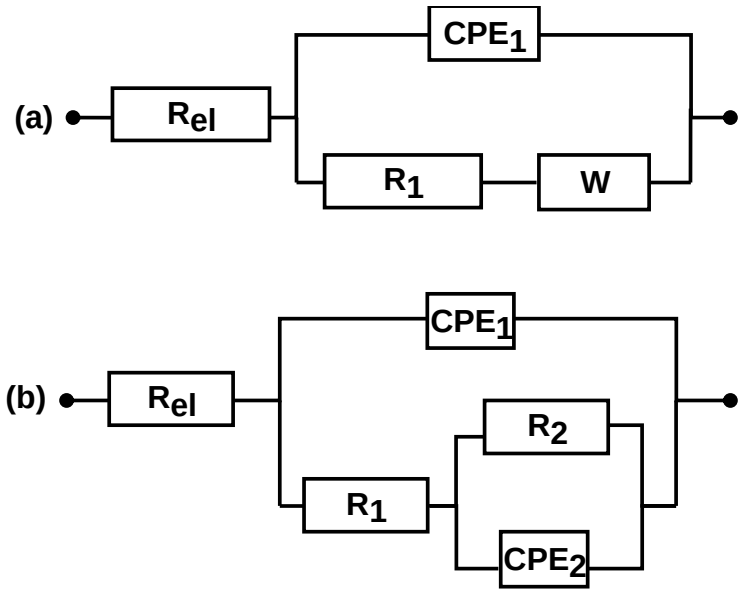

Figure 9. EEC models used to fit EIS data recorded on *(a)* a are 316L SS surface (control sample), and *(b)* on a MUA-modified 316L SS sample.

Figure 8 shows that the agreement between the experimental (symbols) and modeled (lines) data is excellent, demonstrating that the two EECs used indeed give the physical picture of the corresponding two solid/liquid interfaces and processes occurring at them. The corresponding EEC parameter values are presented in Table 0.1.

Table 0.1. EEC parameters obtained by fitting the spectra in Figure 8 using the EECs in Figure 9.

Sample	R_{el} [Ω]	CPE_1 $\times 10^6$ [Ω^{-1} s^n]	n_1	R_1 [kΩ]	$W \times 10^5$ [Ω^{-1} $s^{0.5}$]	$CPE_2 \times 10^6$ [Ω^{-1} s^n]	n_2	R_2 [kΩ]
Bare SS	20.3	46.3	0.89	102	4.8	-	-	-
MUA-modified SS	16.2	41.3	0.92	198	-	3.7	0.87	1831

The values of the exponent *n* of the two CPE elements are close to one, confirming that the constant phase elements indeed represent capacitance. By comparing the CPE_1 values, we can see that when the MUA is present on the surface, the corresponding capacitance decreases slightly. Considering that the decrease is only minor, it could be concluded that the CPE_1 value is governed predominantly by the passive film capacitance, rather than the double-layer capacitance. However, it would be more interesting to compare the relative difference and the corresponding time behavior of corrosion resistance values (R_1 + R_2). For this purpose, the corrosion inhibition efficiency of MUA SAM, η (in %), was calculated by comparing the total corrosion resistance value measured in the presence of MUA SAM on the surface, R_{MUA} (in Ω), to the corresponding resistance value of the bare SS surface, R_o (in Ω) [70]: $\eta = (1 - R_{MUA}/R_o) \times 100\%$.

Figure 10 shows the variation of η with time, and demonstrates that the modification of the SS surface with the MUA SAM increased the corrosion resistance of the surface. In the initial day (*i.e.* after one hour of immersion, day zero), the obtained corrosion inhibition efficiency was 82%, but after one day of immersion it increased to 94% and remained high and statistically constant during the remaining immersion period ($\alpha = 0.05$, $p > 0.28$). The initial lower corrosion inhibition efficiency day zero) indicates that the initially formed MUA SAM was not well packed/structured, thus offering some 'paths' (holes) for the transport of aggressive ions from the bulk solution to the underlying 316L SS surface. However, with the immersion time, the structure of the MUA SAM most likely changed resulting in better resistance to transport of aggressive ions thorough it.

Thus, the EIS measurements presented in Figure 10 demonstrate that the MUA SAM offers high corrosion protection over a prolonged immersion time in an aggressive electrolyte, which is of high importance for the use of a MUA-functionalized 316L SS in various applications where high corrosion resistance of the surface is imperative (coronary stents, dental implants, processing equipment in the dairy, food, and pharmaceutical industries, etc.).

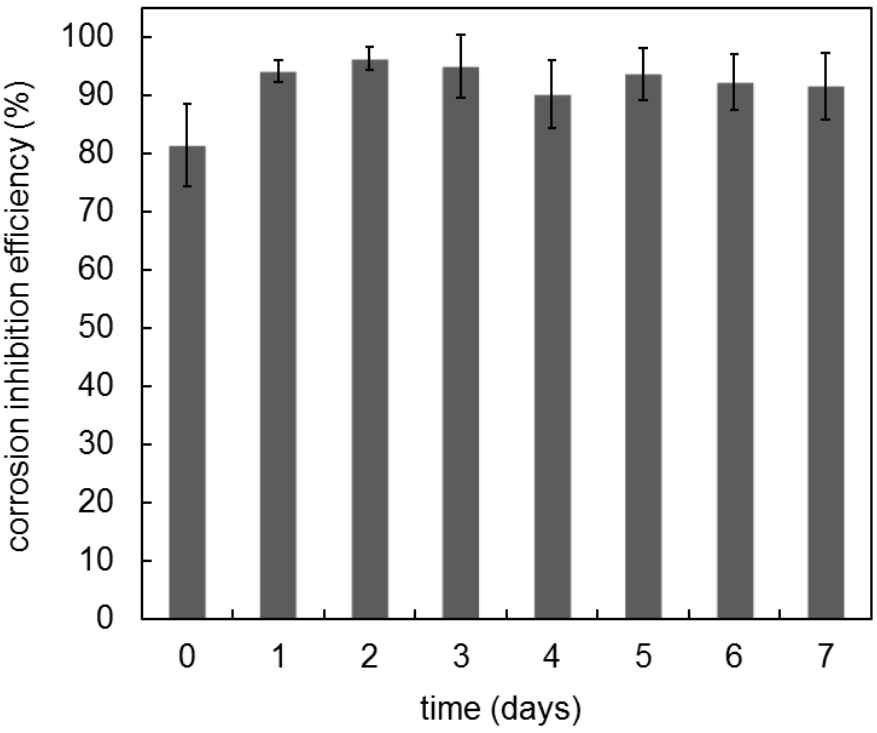

Figure 10. General corrosion inhibition efficiency of a MUA SAM formed on a 316L SS surface measured in PBS (pH = 7.4) and at temperature = 37 °C during seven days of constant immersion, using EIS.

The EIS data demonstrate that that MUA-modified 316L SS surface indeed offers higher corrosion resistance than the bare 316L SS surface, thus proving the hypothesis introduced earlier in the text. The origin of the increased resistance of the MUA-modified surface lies in the presence of a hydrophobic barrier on the 316L SS surface. When the MUA SAM is formed on the 316L SS surface,

the long hydrophobic $–CH_2$ chain presents a barrier for the penetration of solvated aggressive ions to the underlying surface. In this way, corrosion of the 316L SS surface is minimized. Similar results were observed previously in our laboratory, particularly in the inhibition of 316L SS corrosion by a linoleic acid (LA) anion [71] and of carbon steel corrosion by long-chain amino acids [67-69].

4. CONCLUSION

A COOH-terminated alkanethiol (MUA) SAM was successfully formed on a 316L stainless steel surface using an electrochemical method. The stability of the monolayer was assessed by PM-IRRAS, CA, and EIS. XPS demonstrated that the SAM was attached to the stainless steel surface through the MUA sulfur atom, although results also evidenced that some MUA molecules bound to the surface through both the thiol and the carboxylate group, exposing the hydrophobic alkane chain to the surface's exterior The formed SAM was reasonably stable in a corrosive environment over a period of several days, and also withstood the exposure to fluid shear simulating blood circulation. Furthermore, the SAM also showed a substantial thermal stability at elevated temperatures.

ACKNOWLEDGEMENTS
The authors would like to thank the Natural Science and Engineering Research Council of Canada and the Canadian Institutes of Health Research for support of this research, through a Collaborative Health Research Program grant.

References

1. G. Towler and R. Sinnott, *Materials of Construction- Chapter 6*, Butterworth-Heinemann, Boston (2012).
2. Y. Chisti, *Processs Hygiene | Modern Systems of Plant Cleaning*, Elsevier, Oxford (1999).
3. B. O'Brien and W. Carroll, *Acta Biomater.*, 5 (2009) 945.
4. D. Brown, M. Braden, B. E. Causton, E. C. Combe, D. W. Cruickshanks-Boyd, A. M. Fletcher, C. H. Lloyd, J. F. McCabe, M. Miller, H. J. Prosser, N. E. Waters, D. C. Watts, D. F. Williams, A. D. Wilson, and H. J. Wilson, *J. Dent.*, 9 (1981) 271.
5. J. Walczak, F. Shahgaldi, and F. Heatley, *Biomaterials*, 19 (1998) 229.
6. M. Sivakumar and S. Rajeswari, *J. Mater. Sci. Lett.*, 11 (1992) 1039.
7. M. Prikryl, S. C. Srivastava, G. R. Viviani, M. B. Ives, and G. R. Purdy, *Biomaterials*, 10 (1989) 109.
8. M. Huber, G. Reinisch, G. Trettenhahn, K. Zweymuller, and F. Lintner, *Acta Biomater.*, 5 (2009) 172.
9. C. Heintz, G. Riepe, L. Birken, E. Kaiser, N. Chakfe, M. Morlock, G. Delling, and H. Imig, *J. Endovasc. Ther.*, 8 (2001) 248.
10. F. Zhang, E. T. Kang, K. G. Neoh, P. Wang, and K. L. Tan, *Biomaterials*, 22 (2001) 1541.
11. E. De Giglio, M. R. Guascito, L. Sabbatin, and G. Zambonin, *Biomaterials*, 22 (2001) 2609.
12. E. De Giglio, L. De Gennaro, L. Sabbatini, and G. Zambonin, *J. Biomater. Sci., Polym. Ed.*, 12 (2001) 63.
13. T. Laursen, D. J. Johnson, D. T. Amm, and J. E. Haysom, *Mat. Sci. Eng. A-Struct.*, 174 (1994) L13.

14. C. R. Kaufmann, G. Mani, D. Marton, D. M. Johnson, and C. M. Agrawal, *Biomed. Mater.*, 5 (2010) 25008.
15. A. Mahapatro, D. M. Johnson, D. N. Patel, M. D. Feldman, A. A. Ayon, and C. M. Agrawal, *Langmuir*, 22 (2006) 901.
16. A. Raman, M. Dubey, I. Gouzman, and E. S. Gawalt, *Langmuir*, 22 (2006) 6469.
17. C. M. Ruan, T. Bayer, S. Meth, and C. N. Sukenik, *Thin Solid Films*, 419 (2002) 95.
18. G. Shustak, A. J. Domb, and D. Mandler, *Langmuir*, 20 (2004) 7499.
19. G. Shustak, A. J. Domb, and D. Mandler, *Langmuir*, 22 (2006) 5237.
20. S. Meucci, G. Gabrielli, and G. Caminati, *Mat. Sci. Eng. C-Bio. S.*, 8-9 (1999) 135.
21. S. J. Dong and J. H. Li, *Bioelectroch. Bioener.*, 42 (1997) 7.
22. Y. D. Zhao, D. W. Pang, S. Hu, Z. L. Wang, J. K. Cheng, and H. P. Dai, *Talanta*, 49 (1999) 751.
23. K. Sugihara, K. Shimazu, and K. Uosaki, *Langmuir*, 16 (2000) 7101.
24. E. Corte´s, A. A. Rubert, G. Benitez, P. Carro, M. E. Vela, and R. C. Salvarezza, *Langmuir*, 25 (2009) 5661.
25. J. S. Park, A. C. Smith, and T. R. Lee, *Langmuir*, 20 (2004) 5829.
26. C. Vericat, G. A. Benitez, D. E. Grumelli, M. E. Vela, and R. C. Salvarezza, *J. Phys.: Condens. Matter.*, 20 (2008) 184004.
27. T. M. Willey, A. L. Vance, T. van Buuren, C. Bostedt, L. J. Terminello, and C. S. Fadley, *Surf. Sci.*, 576 (2005) 188.
28. J. P. Folkers, P. E. Laibinis, and G. M. Whitesides, *Langmuir*, 8 (1992) 1330.
29. W. J. Li, J. A. Virtanen, and R. M. Penner, *J. Phys. Chem.*, 98 (1994) 11751.
30. P. Lang, Z. Mekhalif, B. Rat, and F. Garnier, *J. Electroanal. Chem.*, 441 (1998) 83.
31. J. G. Van Alsten, Langmuir, 15 (1999) 7605.
32. T. Aqua, H. Cohen, A. Vilan, and R. Naaman, *J. Phys. Chem. C*, 111 (2007) 16313.
33. D. K. Peng and J. Lahann, *Langmuir*, 23 (2007) 10184.
34. H. Ly and J. B. Schlenoff, *Abstr. Pap. Am. Chem. S.*, 210 (1995) 227.
35. J. B. Schlenoff, M. Li, and H. Ly, *J. Am. Chem. S.*, 117 (1995) 12528.
36. I. Thom and M. Buck, *Surf. Sci.*, 581 (2005) 33.
37. G. Mani, D. M. Johnson, D. Marton, V. L. Dougherty, M. D. Feldman, D. Patel, A. A. Ayon, and C. M. Agrawal, *Langmuir*, 24 (2008) 6774.
38. A. Raman and E. S. Gawalt, *Langmuir*, 23 (2007) 2284.
39. S. Omanovic, J. Harvey, and H. Dadafarin,*Modified Stainless Steel Surface and Method for Preparing the Same Using an Electrochemical Process*, Patent Application No.: 61391335, (USA/Canada)
40. J. Harvey, A. Bergdahl, H. Dadafarin, L. Ling, E. C. Davis, and S. Omanovic, *Biotechnol. Lett.*, 34 (2012) 1159.
41. R. Meunier-Prest, G. Legay, S. Raveau, N. Chiffot, and E. Finot, *Electrochim. Acta*, 55 (2010) 2712.
42. A. Hatzor, T. Moav, H. Cohen, S. Matlis, J. Libman, A. Vaskevich, A. Shanzer, and I. Rubinstein, *J. Am. Chem. S.*, 120 (1998) 13469.
43. S. Oyre, W. P. Paaske, S. Ringgaard, S. Kozerke, M. Erlandsen, P. Boesiger, and E. M. Pedersen, *Eur. J. Vasc. Endovasc.*, 16 (1998) 517.
44. S. Schilt, J. E. Moore, Jr., A. Delfino, and J. J. Meister, *J. Biomech.*, 29 (1996) 469.
45. P. J. Elving and M. S. Spritzer, *Talanta*, 12 (1965) 1243.
46. W. Gao, L. Dickinson, C. Grozinger, F. G. Morin, and L. Reven, *Langmuir*, 12 (1996) 6429.
47. A. H. M. Sondag and M. C. Raas, *J. Chem. Phys.*, 91 (1989) 4926.
48. D. L. Allara and R. G. Nuzzo, *Langmuir*, 1 (1985) 45.
49. Y. T. Tao, G. D. Hietpas, and D. L. Allara, *J. Am. Chem. S.*, 118 (1996) 6724.
50. A. Faucheux, A. C. Gouget-Laemmel, C. Henry de Villeneuve, R. Boukherroub, F. Ozanam, P. Allongue, and J. N. Chazalviel, *Langmuir*, 22 (2006) 153.

51. J. A. Harvey, *Covalent attachment of fibronectin to 316L stainless steel using amine and carboxylic acid alkanethiol self-assembled monolayers: Applications for coronary artery stents.*, M.Eng. Thesis, McGill University (Canada) (2009), 122.
52. M. Futamata, *J. Electroanal. Chem.*, 550 (2003) 93.
53. R. Arnold, W. Azzam, A. Terfort, and C. Woll, *Langmuir*, 18 (2002) 3980.
54. J. Maciel, M. C. Martins, and M. A. Barbosa, *J. Biomed. Mater. Res. A*, 94 (2010) 833.
55. M. Volmer-Uebing and M. Stratmann, *Appl. Surf. Sci.*, 55 (1992) 19.
56. Z. Mekhalif, F. Laffineur, N. Couturier, and J. Delhalle, *Langmuir*, 19 (2003) 637.
57. Y. H. Wang, Q. Yu, Y. Zhang, Z. R. Guo, N. Gu, and K. D. Wesche, *Appl. Surf. Sci.*, 229 (2004) 377.
58. C. M. Yam, M. Deluge, D. Tang, A. Kumar, and C. Cai, *J. Colloid Interface Sci.*, 296 (2006) 118.
59. H. Wang, S. Chen, L. Li, and S. Jiang, *Langmuir*, 21 (2005) 2633.
60. C. D. Bain, E. B. Troughton, Y. T. Tao, J. Evall, G. M. Whitesides, and R. G. Nuzzo, *J. Am. Chem. S.*, 111 (1989) 321.
61. Y. Arima and H. Iwata, *Biomaterials*, 28 (2007) 3074.
62. L. C. Xu and C. A. Siedlecki, *Biomaterials*, 28 (2007) 3273.
63. Y. L. Lee and C. Y. Chen, *Appl. Surf. Sci.*, 207 (2003) 51.
64. A. Shahryari, F. Azari, H. Vali, and S. Omanovic, *Phys. Chem. Chem. Phys.*, 11 (2009) 6218.
65. F. S. Shieu, M. J. Deng, and S. H. Lin, *Corros. Sci.*, 40 (1998) 1267.
66. C. M. Xu, Y. H. Zhang, G. X. Cheng, and W. S. Zhu, *Chin. J. Chem. Eng.*, 14 (2006) 829.
67. S. Ghareba and S. Omanovic, *Corros. Sci.*, 52 (2010) 2104.
68. S. Ghareba and S. Omanovic, *Electrochim. Acta*, 56 (2011) 3890.
69. S. Ghareba and S. Omanovic, *Corros. Sci.*, 53 (2011) 3805.
70. M. Özcan, İ. Dehri, and M. Erbil, *Appl. Surf. Sci.*, 236 (2004) 155.
71. S. Omanovic and S. G. Roscoe, *Corrosion*, 56 (2000) 684